Jets and quantum chromodynamics

I.M. Dremin

Lebedev Physical Institute, Moscow

The brief survey of the strong interaction theory is presented. The jet phenomenon is treated. The basic principles of quantum chromodynamics and phenomenological approaches to strong interaction processes are described. Their predictions and recent achievements in describing experimental data at high energies are considered.

BRIEF HISTORICAL OVERVIEW

Initial stage

$p,\ n \to A$ (Heisenberg; Ivanenko, 1932)

pn-interaction (Tamm, 1934)

Pion (Yukawa, 1935)

Intensive period

Statistical model (Fermi, 1950)

ID(F.,P.,53) → Hydrodynamical model (Landau, 1953)

One-pion exchange model (Dremin, Chernavsky, 1959)

Reggeons (Regge, 1960; Gribov, 1961)

Multiperipheral model (Amati, Fubini, Stanghellini, Tonin, 1962)

Quarks (Gell-Mann; Zweig; Ne'eman, 1964)

Partons (Feynman)→Scaling (Bjorken), 1969

QCD (AF→Gross, Wilczek; Politzer, 1973)

Lattice (Wilson, 1974)

DGLAP-equations (Dokshitzer, 1977; Gribov, Lipatov, 1972(EM); Altarelli, Parisi, 1977)

BFKL-equations (Balitsky, Fadin, Kuraev, Lipatov, 1977)

JETS (U.K.V.,79) → Lund model (Andersson, 1977)

Condensate+Sum rules (Shifman, Vainshtein, Zakharov, 1979)

Dual parton model (Capella, Sukhatme, Tan, Tran, 1979)

Multireggeon model (Kaidalov, Ter-Martirosyan, 1982)

AA (McL.,93) →

QCD Lagrangian

$$L = i\Sigma_q \bar{\psi}_q^a (\nabla_\mu \gamma_\mu + i m_q)\psi_q^a - \frac{1}{4} G_{\mu\nu}^n G_{\mu\nu}^n,$$

$$\nabla_\mu = \partial_\mu - ig\frac{\lambda^n}{2} A_\mu^n,$$

$$G_{\mu\nu}^n = \partial_\mu A_\nu^n - \partial_\nu A_\mu^n + g f^{nml} A_\mu^m A_\nu^l.$$

ψ_q^a and A_μ^n are quark and gluon fields, a=1,2,3; n, m, l=1,2,...8 are color indices, λ^n and f^{nml} are Gell-Mann matrices and f-symbols, m_q are bare (current) quark masses, quark flavors are $q = u, d, s, c, b, t$.

Asymptotic freedom

Coupling strength: $\alpha_s(\mu) = \frac{g^2}{4\pi} = \frac{6\pi}{(33-2n_f)\ln\frac{\mu}{\Lambda}}$

High energies (μ) and high momentum transfers; short distances. Perturbation theory. (Fig. 1)

Confinement

Low energies; static properties; condensates. Non-perturbative approach. Phenomenology. Hadrons are not the eigenstates of QCD.

Soft hadronization

Multiparticle production is the main process at high energies ((?) partons $\rightarrow$ hadrons). Local parton-hadron duality (LPHD) hypothesis. Parton fragmentation functions - phenomenology.

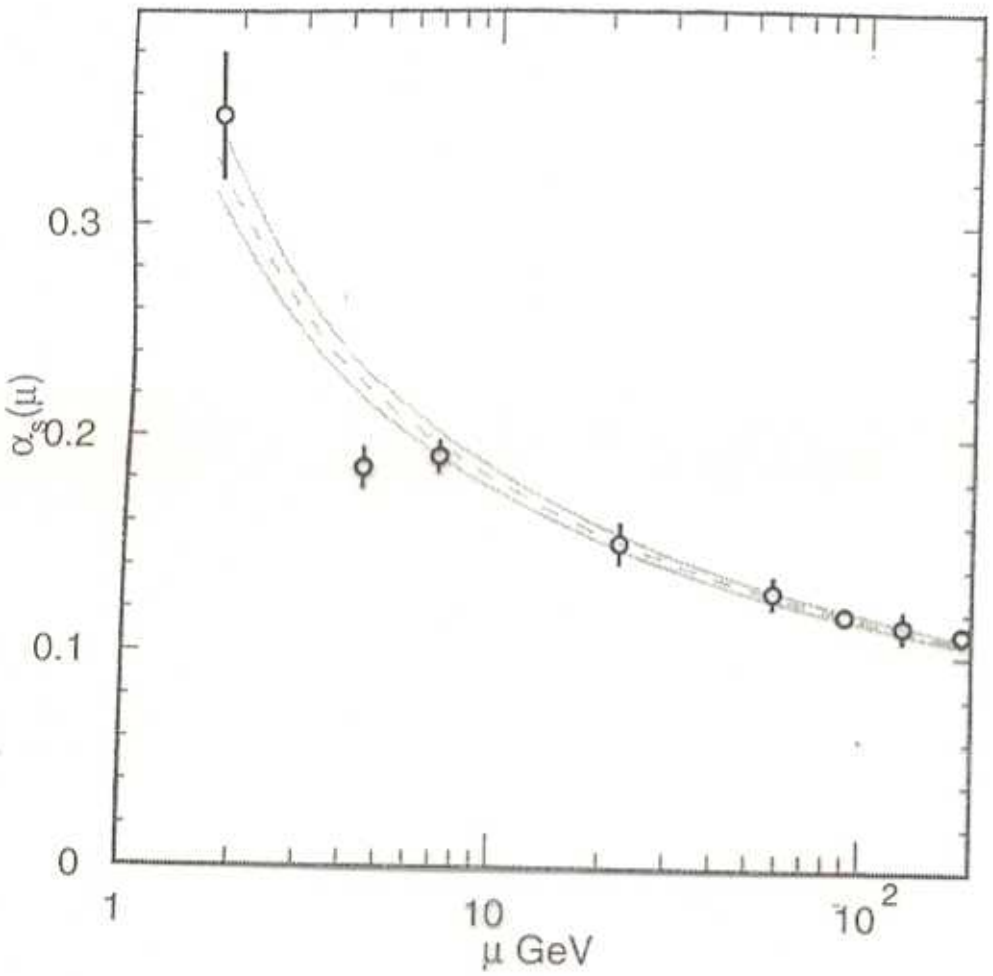

Fig. 1

Extensive period

Analytic calculations and Monte-Carlo models for

e^+e^-, ep, $pp(p\bar{p})$, pA, AA

e^+e^- - **annihilation**

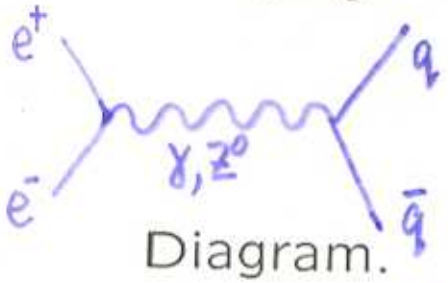

Diagram.

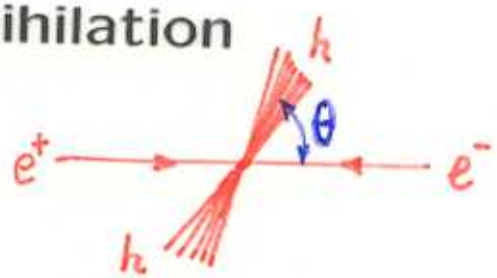

Process.

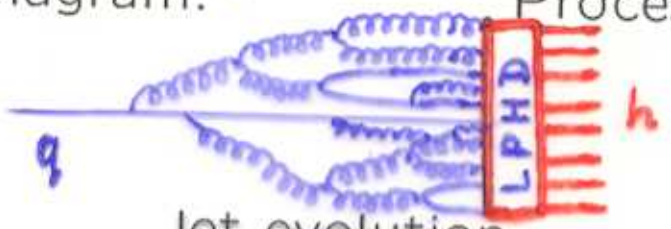

Jet evolution.

Early days

1. Jets (?)

No isotropy; sphericity, spherocity, thrust

2. Spin (?)

$\frac{d\sigma}{d\theta} \propto 1 + \cos^2\theta \rightarrow$spin 1/2 $\rightarrow$quarks

θ is the angle between jet direction and collision axis of e^+e^-.

3. Quarks (?)

$$R = \frac{\sigma_{tot}^{e^+e^-\rightarrow h}}{\sigma^{e^+e^-\rightarrow\mu^+\mu^-}} = 3\cdot\sum_{q=1}^{n_f} e_q^2$$

e_q are electric charges of quarks.

JET STUDIES

DGLAP equations

Symbolically:
EVOLUTION = FISSION - FUSION, i.e.

$$G' = \int d\Omega \alpha_s K [G \otimes G - G]$$

The kernel (weight) $\alpha_s K$ is determined by the QCD Lagrangian.
The integration is over the available phase space Ω.
System of two non-linear integro-differential equations for quarks and gluons.
Their solutions in higher order perturbative approximations improve agreement with experiment.
Hadron distributions are obtained from those for partons (quarks, gluons) with LPHD and hadronization phenomenology.

Comparison with experiment

1. Multiplicities

a. Energy dependence of mean values

$\bar{n} \propto \exp c\sqrt{\ln s}, \quad s = E^2_{c.m.}$ (Fig. 2) (slopes).

Peripheral & Feynman plateau $\bar{n} \propto \ln s$;
hydrodynamics & fixed coupling QCD $\bar{n} \propto s^a$.

b. Ratio of mean multiplicities in gluon and quark jets

$r_0 = C_V/C_F = 2.25 \rightarrow r_{exp} \approx 1.5$ (Fig. 3)

higher perturbative effects and hadronization.

c. Shapes of multiplicity distributions

Moments, correlations, oscillating cumulants $\rightarrow$ analogy with virial coefficients, superconductivity, superfluidity. (Fig. 4)

2. Rapidity distributions

Rapidity: $y = \ln \frac{E+p_z}{\sqrt{p_T^2+m^2}}$.

No Feynman plateau (dn/dy=const)

$\rightarrow$ maximum, shape (Fig. 5)

$\rightarrow$ energy dependence (Fig. 6)

different processes

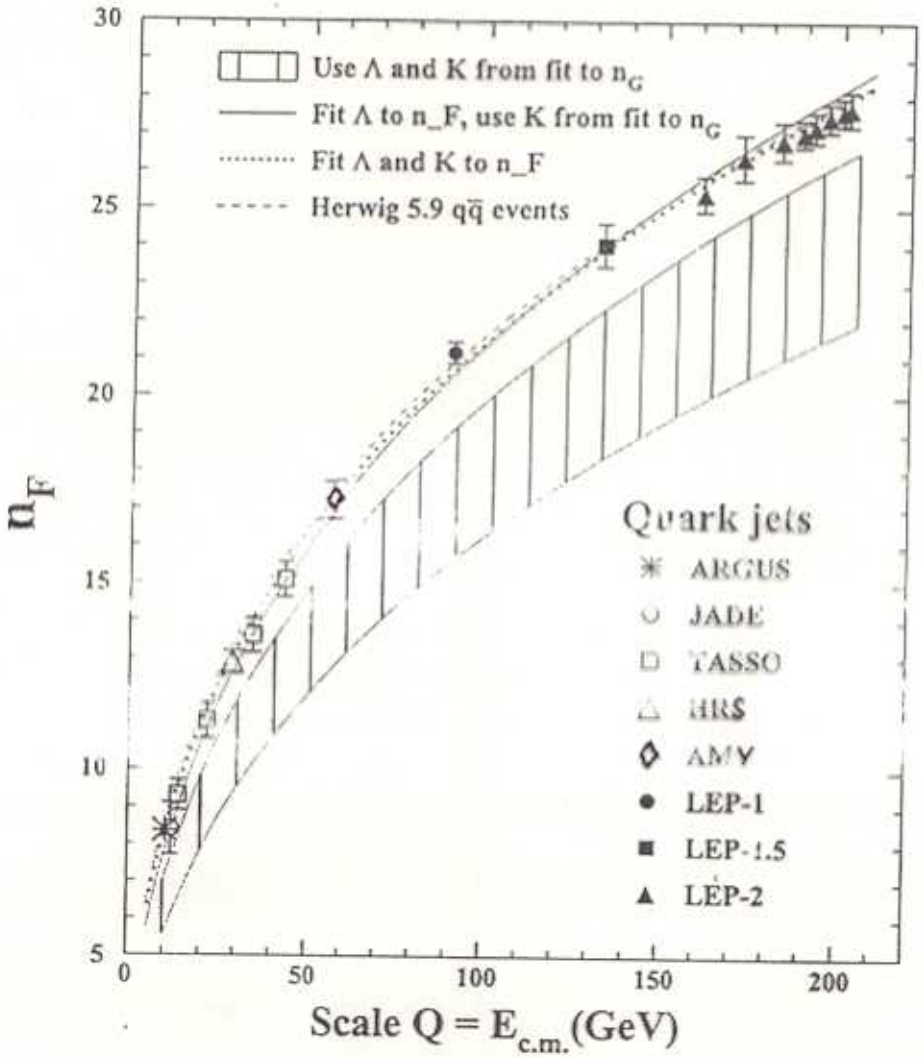

- Mueller
- Webber (−)
- Dremin, Nechitailo
- Capella, Dremin, Gary, Nechitailo, Tran Thanh Van

Fig. 2

$r_{ch.} = \frac{\langle n_{ch.} \rangle_{gluon}}{\langle n_{ch.} \rangle_{quark}} = 1.51 \pm 0.02 \pm 0.05$

$E_{jet} \simeq 41.6$ GeV

$E_{jet} = 80$ GeV

$r_{ch} = 1.548 \pm 0.042$

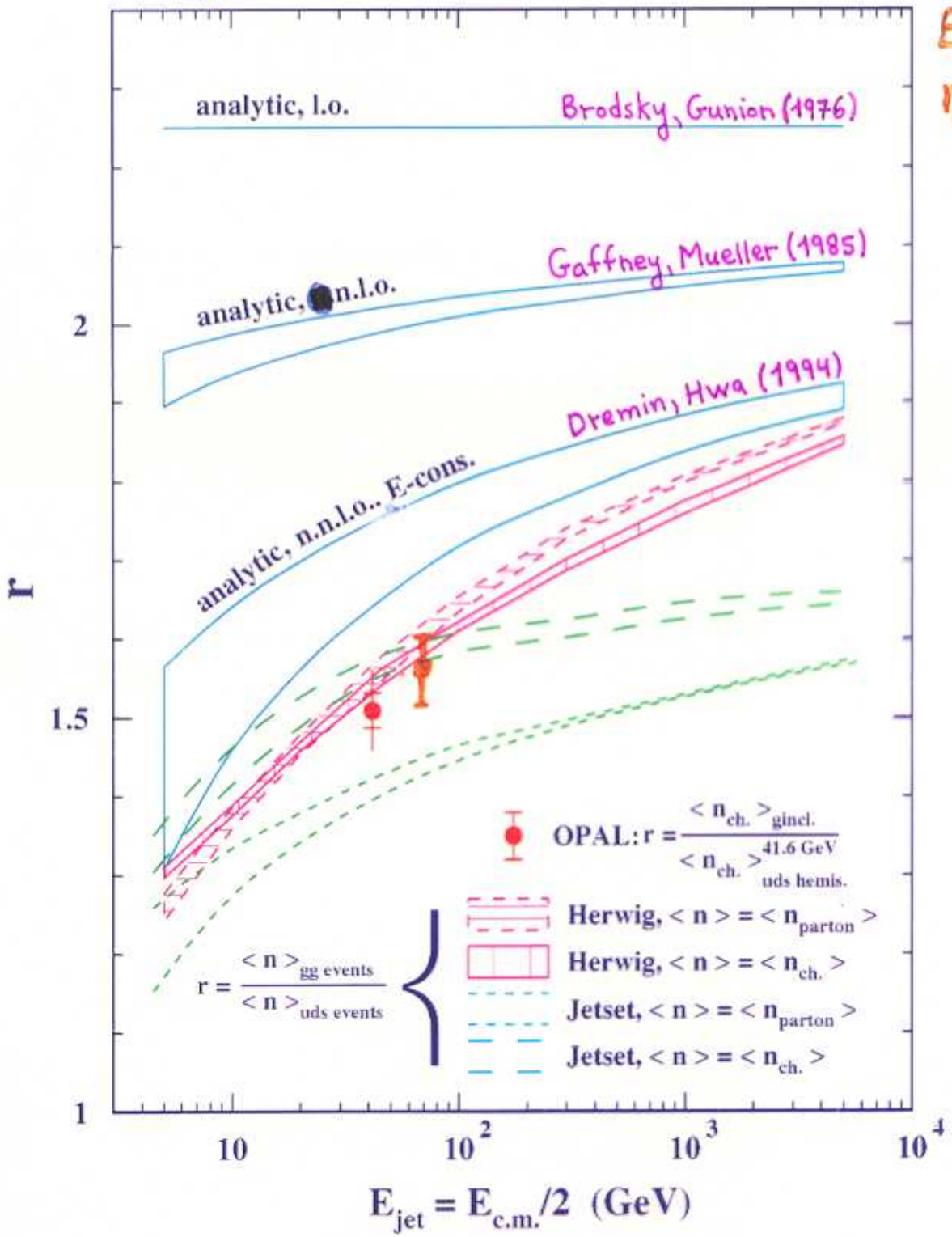

Fig. 3

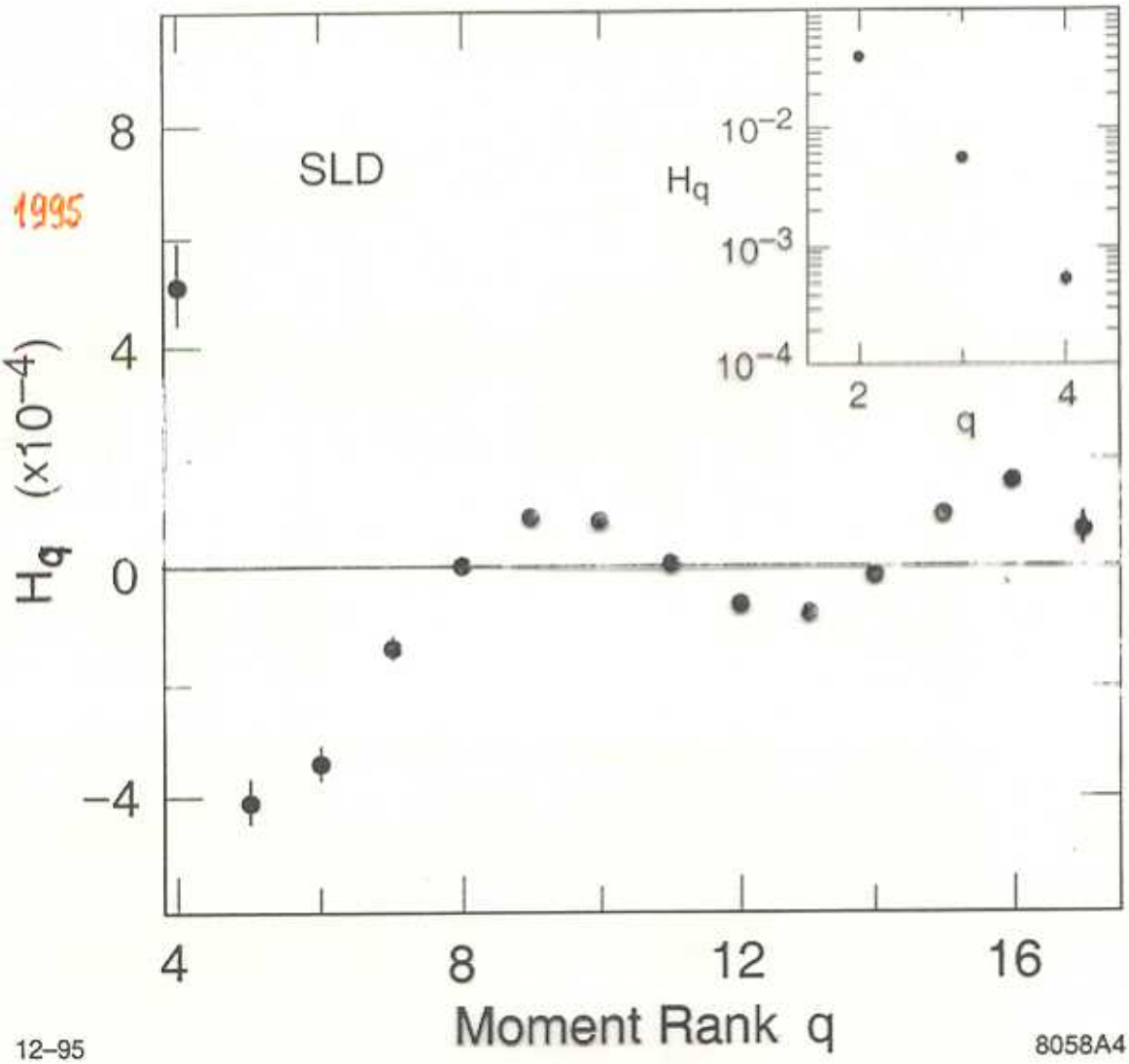

- Dremin (93)
- Dremin, Nechitailo (93)
- Lupia (98)

Fig. 4

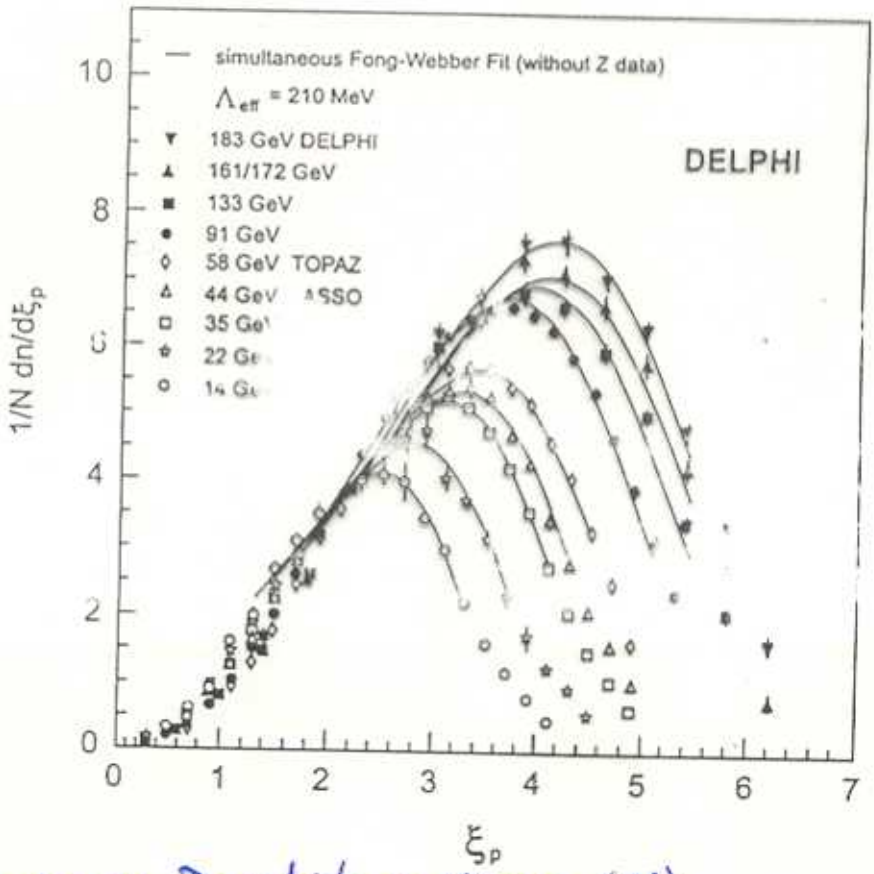

- Azimov, Dokshitzer, Khoze (82)
- Dokshitzer, Fadin, Khoze (82,83)
- Bassetto, Ciafaloni, Marchesini, Mueller (82)

Fig. 5

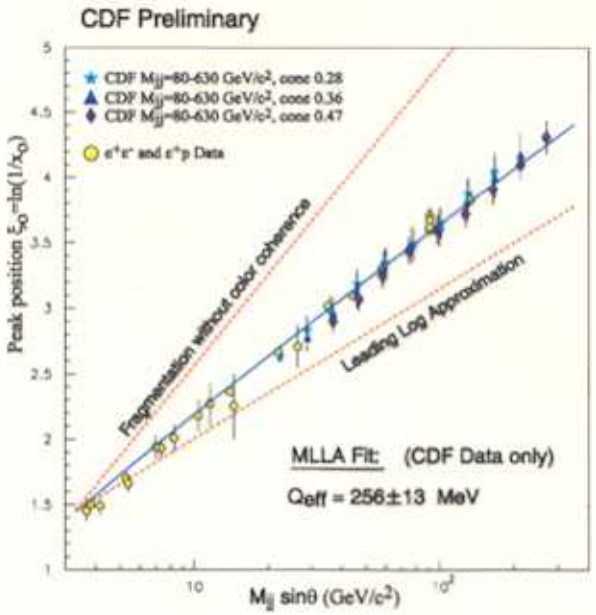

Figure 10: Peak position ξ^* of the inclusive ξ distribution plotted against di-jet mass $\times$ $\sin(\Theta)$ in comparison with the MLLA prediction (central curve); also shown are the double logarithmic approximation (lower curve with asymptotic slope $\xi^* \sim Y/2$) and expectation from cascade without coherence. Result by CDF Collaboration.[92]

data at full angle $\Theta = \pi/2$ from e^+e^- and ep collisions whereby the variable $Y = \ln(P \sin\Theta/Q_0)$ has been used. The data scatter around the expected curve (79) for $n_f = 3$. Taking instead the scaling variable $Y = \ln(2P \sin(\Theta/2)/Q_0)$ the full angle data would be shifted to the right by a factor $2\sin(\pi/4) \sim 1.4$. This would correspond essentially to a change of the next-to-next-to-leading order term in (79) but would not change the slope.

The slope is nicely confirmed and the leading DLA contribution ($\xi^* \sim Y/2$) is shown for comparison as the lower curve in Fig. 10, adjusted in height; the upper curve represents the spectrum for the incoherent cascade which peaks near the maximum ($\xi^* \sim Y$). Apparently the data support the prediction from the parton cascade with suppression of soft particles due to coherent gluon emission in a large energy range $2E_{jet} \sin\Theta \sim 4 - 300$ GeV.

The analytical results for the particle spectrum near the soft limit (90) are nicely confirmed by the data. In these calculations the model (35) for mass effects has been used. The experimental data from the available range

Fig. 6

3. Phase-space structure: intermittency, fractality

Analogy with turbulence in hydrodynamics,
self-similarity at different scales.
Fixed coupling $\rightarrow$ scaling, monofractal,
linear behavior of moments in
log(moment)-log(bin size) plot;
QCD running coupling $\rightarrow$ multifractal,
curvature in log – log plot (Fig. 7).

4. 3-jet events, subjets

Color coherence $\rightarrow$ different suppression of
particle flows between different jets, correlations.
(Fig. 8)

5. Heavy quarks

Dead-cone (ring-like) structure of gluon emission.
QED analogy. (Fig. 9)

6. Jet universality

Jet properties in different processes.
Structure functions (pdf) for hadrons.

V6 22

"Genuine" multiplicity correlations in ring regions

$$F_q \sim (\delta y)^{-\phi_q} \; ; \quad \ln \frac{F_q(z)}{F_q(0)} = \phi_q \ln \frac{\theta_0}{\delta\theta} = \phi_q z = (q-1) d_q z \; ;$$

ϕ_q: intermittency index; d_q: anomalous dimension

fixed α_s = const

d_q = const (z) - mono-fractal

$d_q = d_q(z)$ - multi fractal

↓ running α_s

$d_q = D - D_q$, $D = 1$ ↓ Renyi dimens.

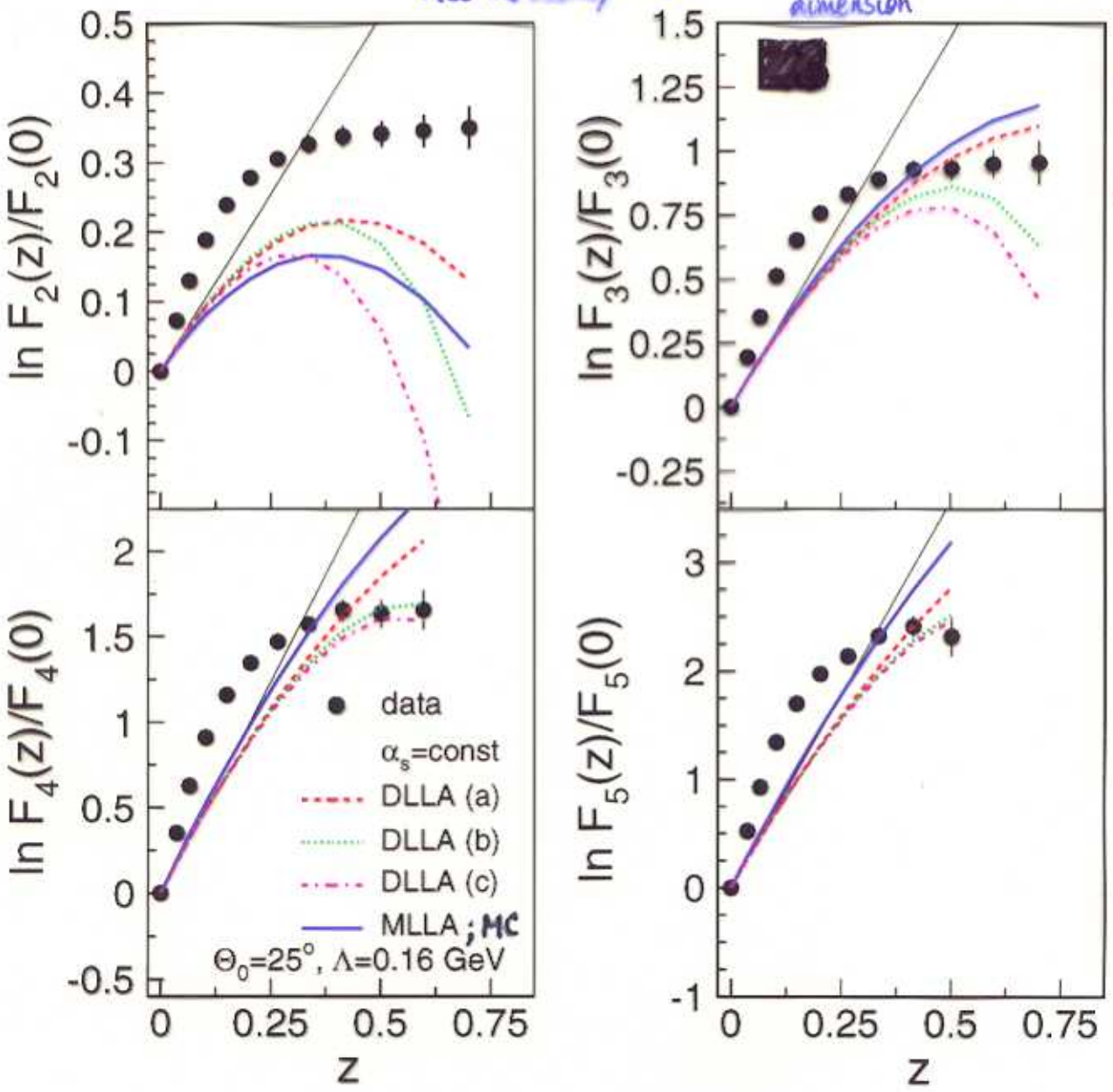

QCD:
- (a) Dokshitzer, Dremin (93)
- (b) Brax, Peschanski (94)
- (c) Ochs, Wosiek (92,93)

- Bialas, Peschanski (86)
- Dremin (87)

$\Lambda = 0.16$ GeV

disagreement for $\Lambda = 0.16$ GeV ($n_f = 3$)

Fig. 7

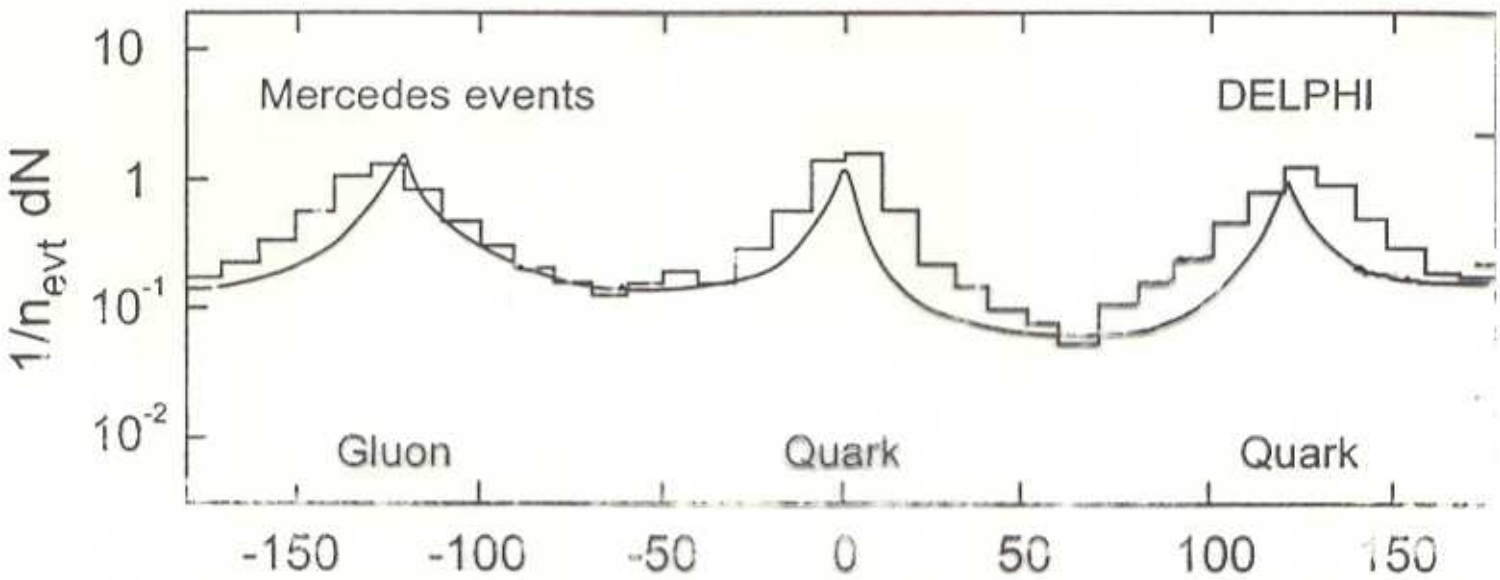

- Andersson, Gustafson, Sjöstrand (80)
- Azimov, Dokshitzer, Khoze, Troyan (85,86)

Fig. 8

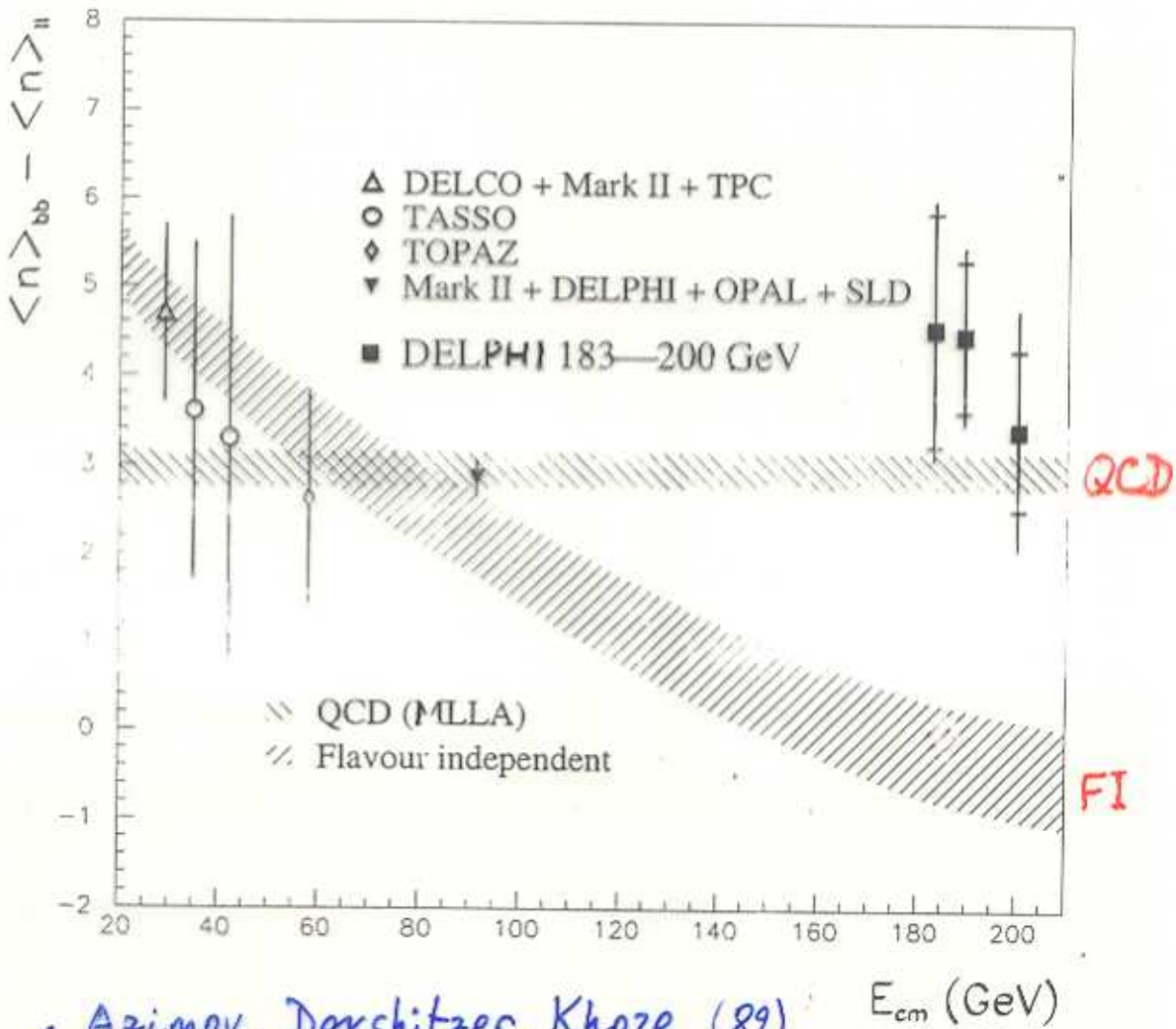

- Azimov, Dokshitzer, Khoze (82)
- Dokshitzer, Fadin, Khoze (82,83)
- Petrov, Kisselev (88,95)
- Dremin (79,81) – em

Fig. 9

QCD factorization theorem

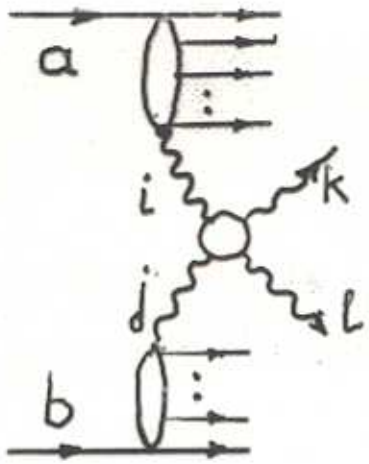

$$d\sigma_{ab}^{kl} \sim \int dx_i dx_j f_a^i(x_i, \mu^2) f_b^j(x_j, \mu^2) d\sigma_{ij}^{kl}$$

$f_a^i(x_i, \mu^2)$ are distributions of partons i in a hadron a, μ is the scale of the hard interaction.

PQCD can predict by evolution equations μ^2 dependences of pdfs. Their x-dependences are determined from experimental data.

Main source of information on pdfs : DIS of leptons on protons and nuclei.

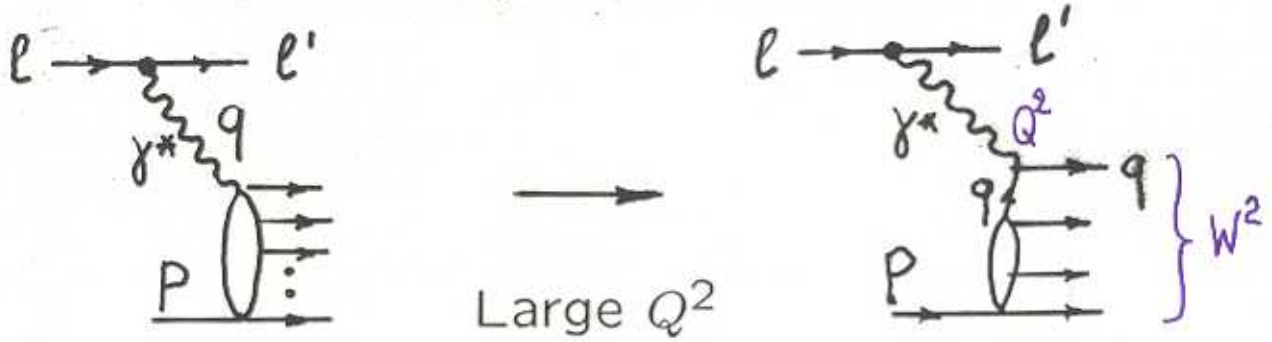

$$x = \frac{Q^2}{2pq}, \quad 2pq = W^2 + Q^2 - m_N^2$$

Cross sections $\frac{d\sigma}{dxdQ^2}$ are described in terms of two structure functions F_2, F_L.

The function F_2 is related to the total cross section of the virtual photon-proton interaction.

$$\sigma^{(tot)}_{\gamma^* p}(W^2, Q^2) = \frac{4\pi^2 \alpha^2_{e.m.}}{Q^2} F_2(x, Q^2)$$

For large Q^2

$$F_2 = \sum_i e_i^2 (q_i(x, Q^2) + \bar{q}_i(x, Q^2))x$$

F_2 is measured in a broad region of x, Q^2. (Fig.10)

Distributions of quarks, antiquarks and gluons in hadrons were determined. (Fig.11)

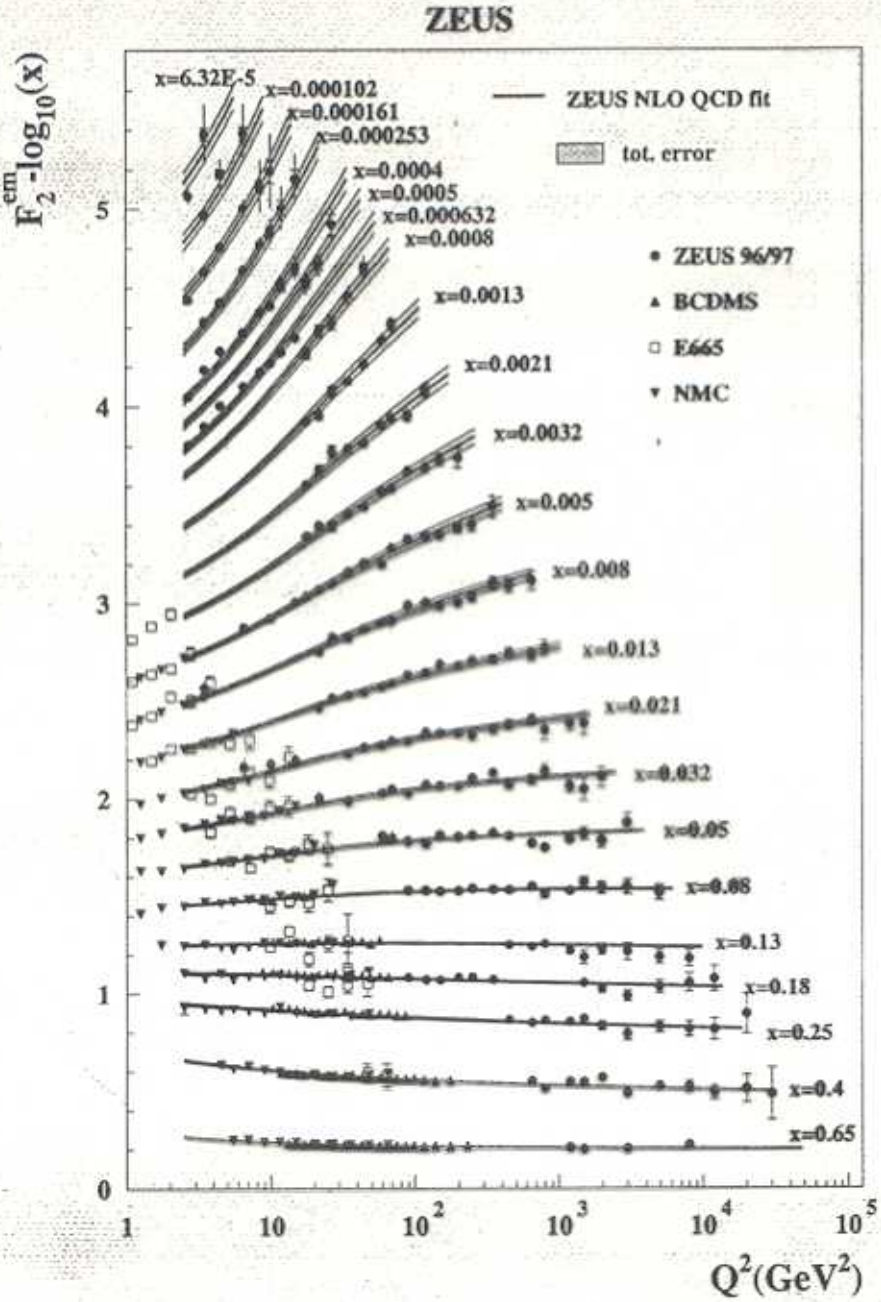

Figure 10: *The ZEUS-S NLO QCD fit compared to ZEUS 96/97 and proton fixed-target F_2 data. The error bands are defined in the caption to Fig. 1.*

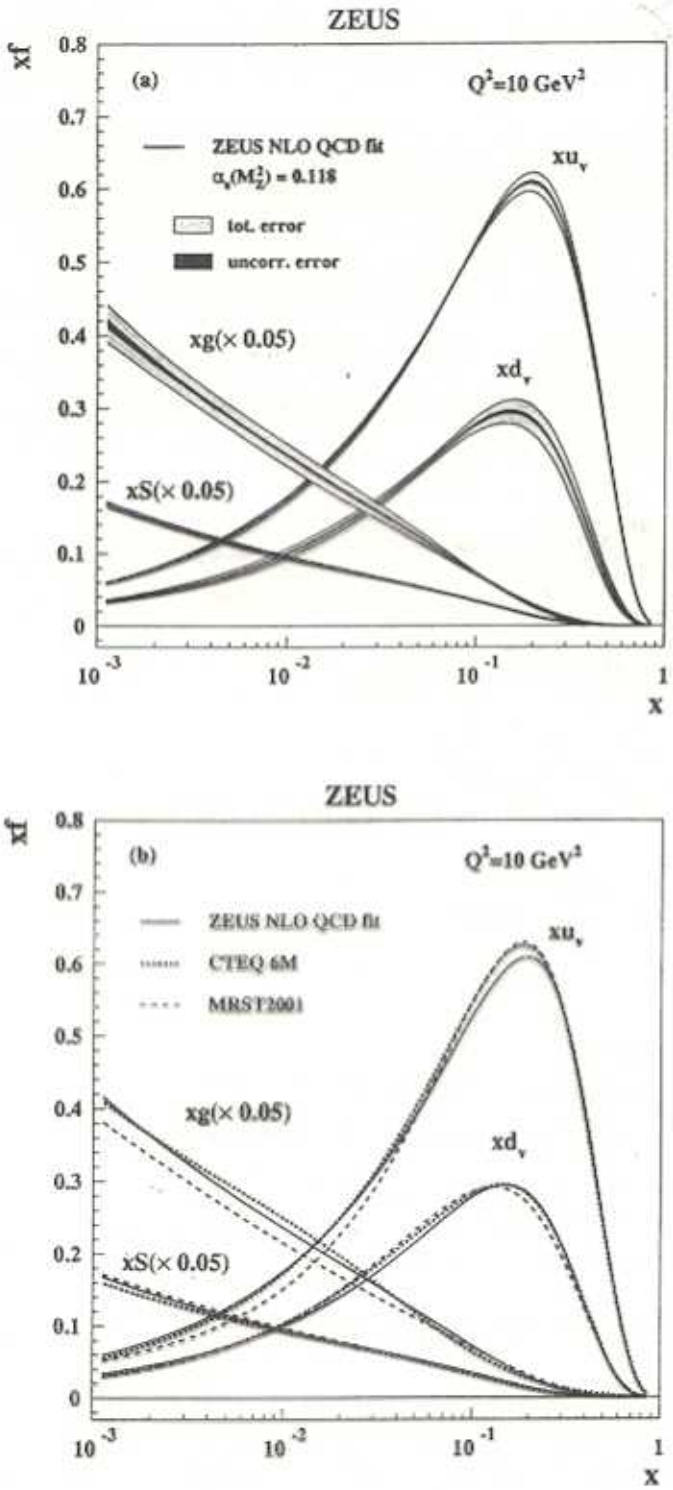

Figure 13: *(a) The gluon, sea, u and d valence distributions extracted from the standard ZEUS-S NLO QCD fit at $Q^2 = 10$ GeV^2. The error bands in this figure show the uncertainty from statistical and other uncorrelated sources separately from the total uncertainty including correlated systematic uncertainties. (b) The gluon, sea, u and d valence distributions extracted from the ZEUS-S NLO QCD fit at $Q^2 = 10$ GeV^2, compared to those extracted from the fits MRST2001 [5] and CTEQ6 [6].*

Several groups carry out a global analysis of data on hard processes (CTEQ, MRST,..).

Production of jets in hadronic interactions

New data from Tevatron Run II. (Fig.12)

QCD well describes hard processes in hadronic interactions.

Small-x physics

Fast increase of structure functions as $x \to 0$.

$$F_2(x, Q^2) \sim (1/x)^{\lambda(Q^2)}$$

$\sigma^{(tot)}_{\gamma^* p}(W^2, Q^2)$ increases with energy much faster than $\sigma^{(tot)}_{pp}$. (Fig.13)

This fast increase can not continue as $x \to 0$ (problems with unitarity).

Very large densities of partons (especially gluons) at high energies ($x \to 0$) due to quark-gluon cascade.(Fig.14)

DØ, M. Wobisch

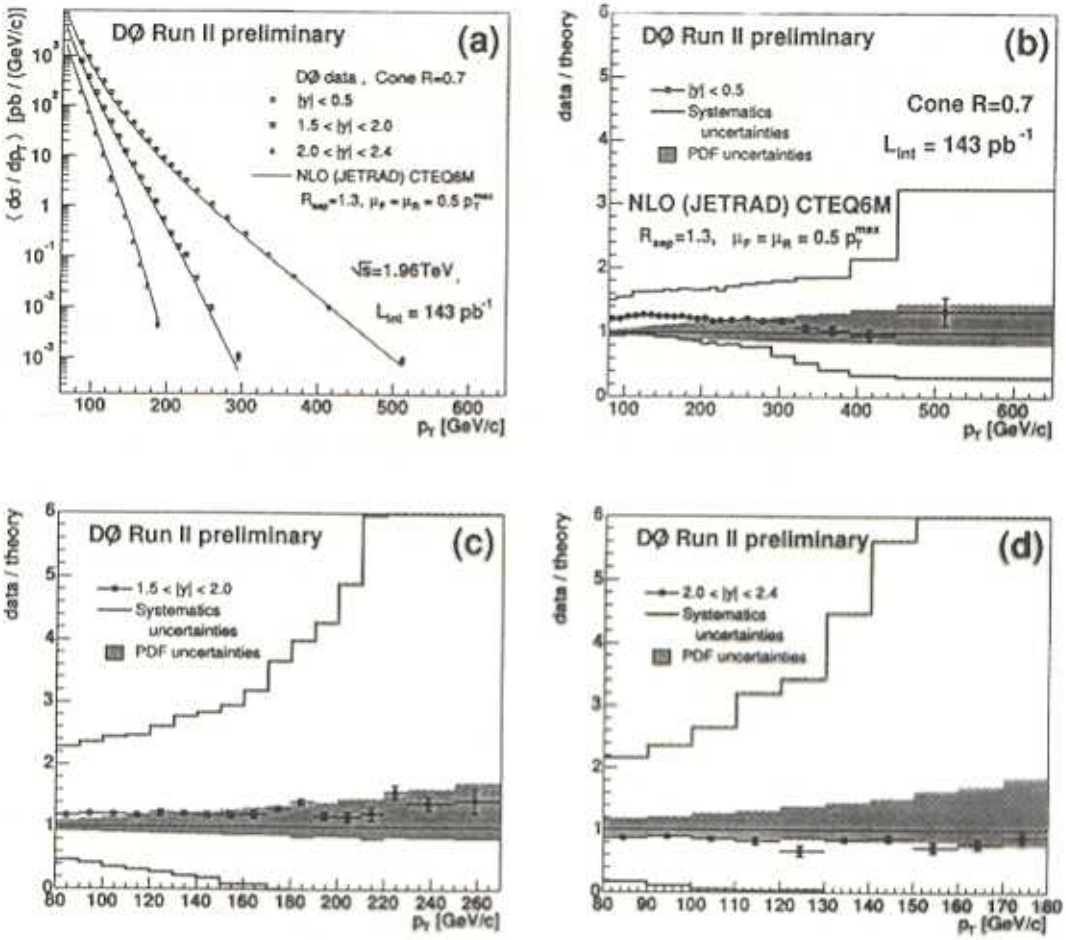

FIGURE 2. The inclusive jet cross section as a function of p_T in different rapidity regions (a). Only statistical errors are shown. Figures (b), (c), (d) show the ratios of data and the NLO pQCD predictions. The error bars indicate the statistical errors and the total experimental uncertainty is displayed by the lines. Theoretical uncertainties due to the PDFs are shown as the shaded bands.

Inclusive Jet and Dijet Jet Cross Sections

The inclusive jet cross section is measured as a function of p_T and y. Fig. 2 (a) shows the p_T dependence of the inclusive jet cross section in three rapidity regions in the range $0 < |y| < 2.4$ (with statistical errors only). The cross section is falling by more than six orders of magnitude between $p_T = 100\,\text{GeV}$ and $p_T = 500\,\text{GeV}$. At forward rapidities the p_T dependence is much stronger. Next-to-leading order (NLO) pQCD predictions are overlaid on the data. The NLO calculations [6] were computed for renormalization and factorization scales $\mu_r = \mu_f = 0.5\,p_T^{\max}$ using the CTEQ6M [7] PDFs and $\alpha_s(M_Z) = 0.118$. The maximum distance of particles within a jet was limited to $\Delta R < R_{\text{sep}} \cdot R_{\text{cone}}$ with $R_{\text{sep}} = 1.3$ [8]. The ratio of data over theory is shown in Figs. 2 (b), (c), (d). Uncertainties in the NLO calculations due to the PDFs are indicated by the grey bands; the experimental uncertainties are displayed as lines. The latter increase with p_T, especially at large rapidities. Theory has good agreement with data given the large

γ^*p cross section at high energy

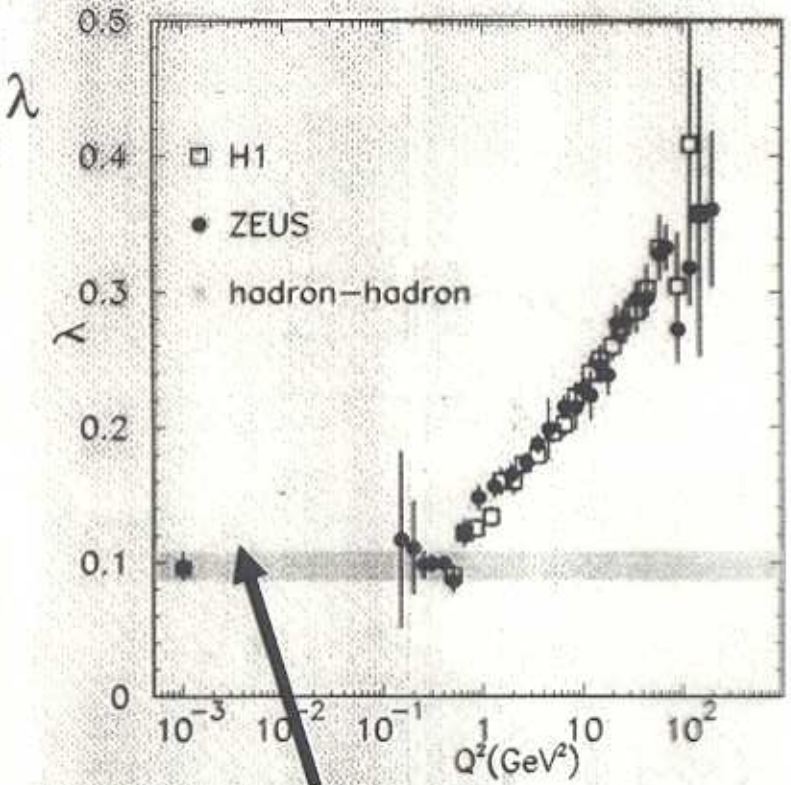

soft Pomeron (p-p) intercept

σ (pp) ~ $s^{0.08} = s^{\alpha(0)-1}$ *at high energy*

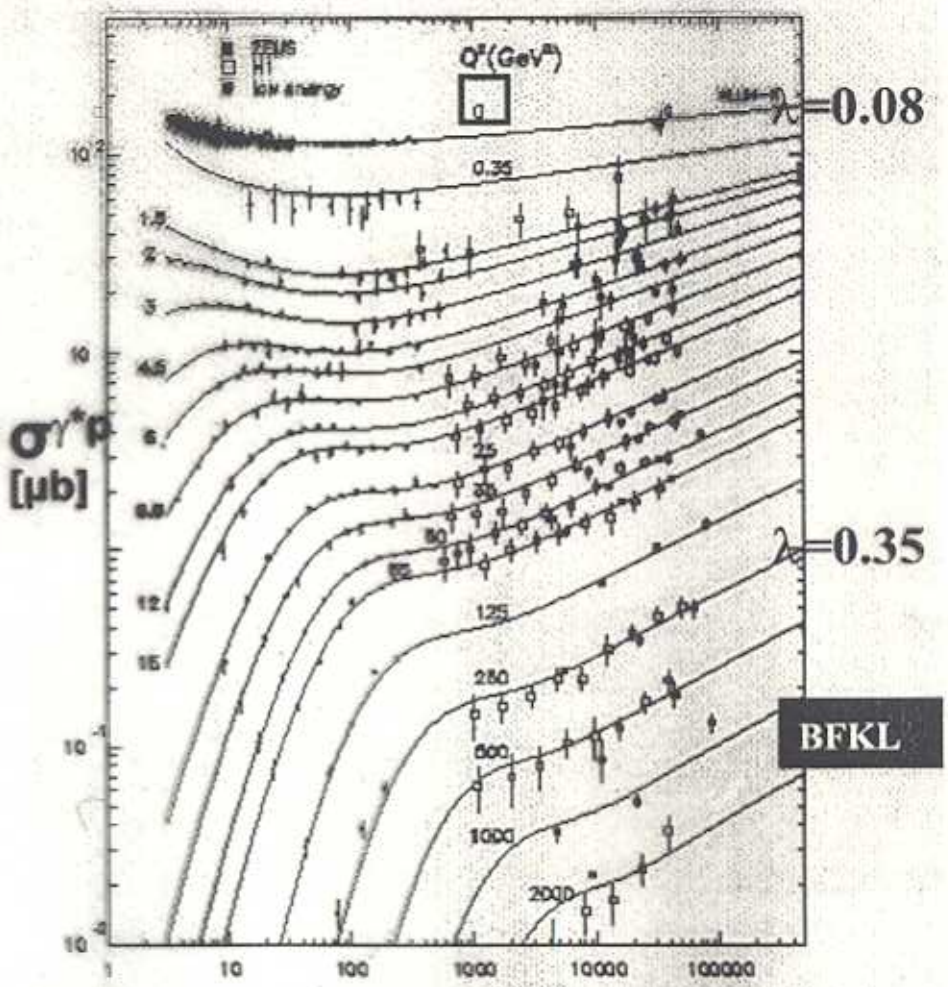

$$\sigma^{\gamma^*p}(W^2) \sim F_2(W^2,Q^2)/Q^2 \sim s^{\lambda}$$

Fig. 13.

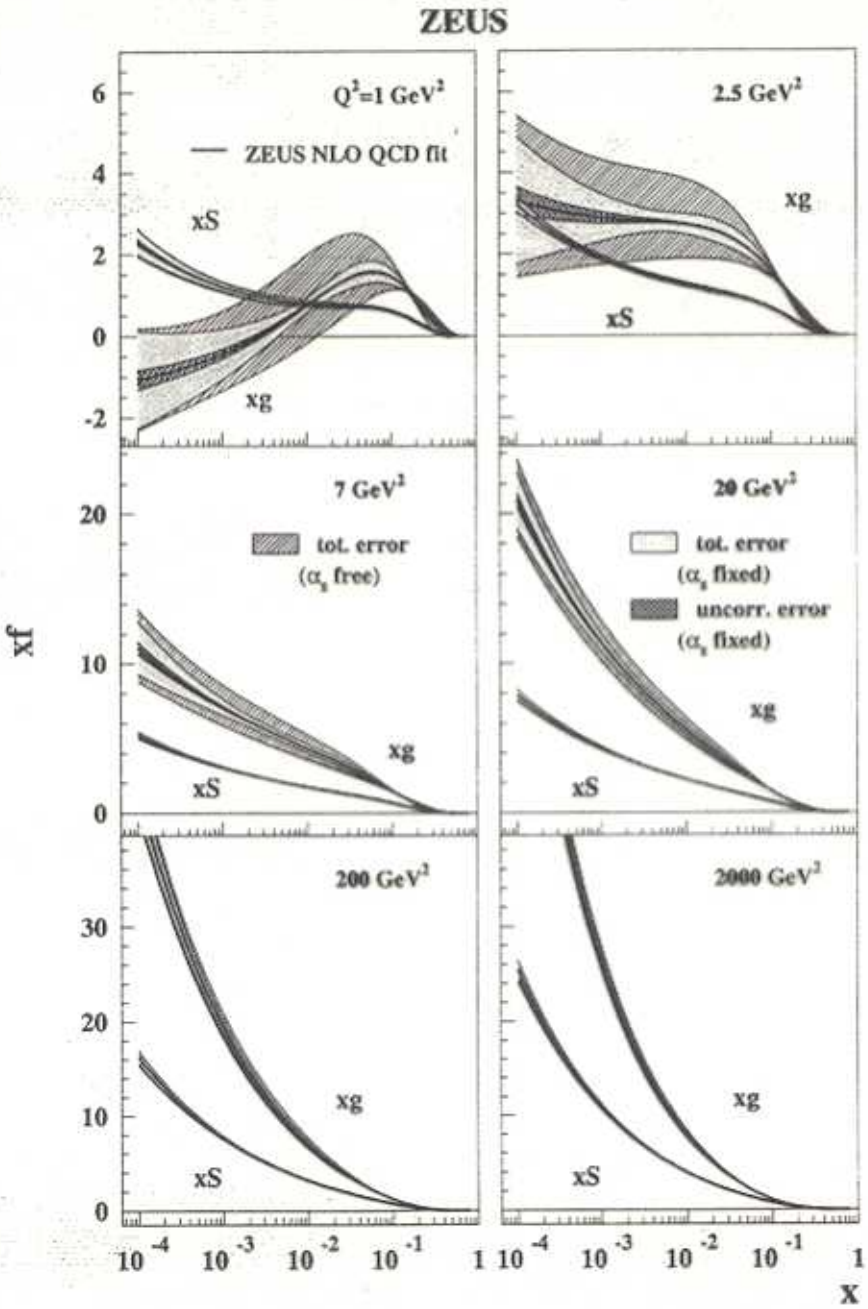

Figure 16: *Comparison of the gluon and sea distributions from the ZEUS-S NLO QCD fit for various Q^2 values. The error bands are defined in the caption to Fig. 6.*

Nonlinear effects in the system (fusion of partons) should lead finally to a "saturation" of parton densities in the limit $x \to 0$.

"Saturation" extends to higher scales Q_s^2 as energy increases. Hopes to calculate these effects in PQCD (L.Gribov. E.Levin. M.Ryskin; A.Mueller, L.McLerran et al.).

These unitarity effects for distributions of partons are important for future hadronic colliders and cosmic rays. $x_1 x_2 = M_\perp^2/s$

For nuclei the nonlinear effects are enhanced: density of partons at given impact parameter $\sim A^{1/3}$.

Shadowing of partons is clearly seen in the structure functions of nuclei for $x \ll 1/(m_N R_A)$. (Fig.15)

It can be calculated using Gribov-Glauber approach for scattering of virtual photons on nuclei and the information on diffractive dissociation of a virtual photon in $\gamma^* p$ collisions.

Important role of large distance, nonperturbative dynamics.

CKMPT

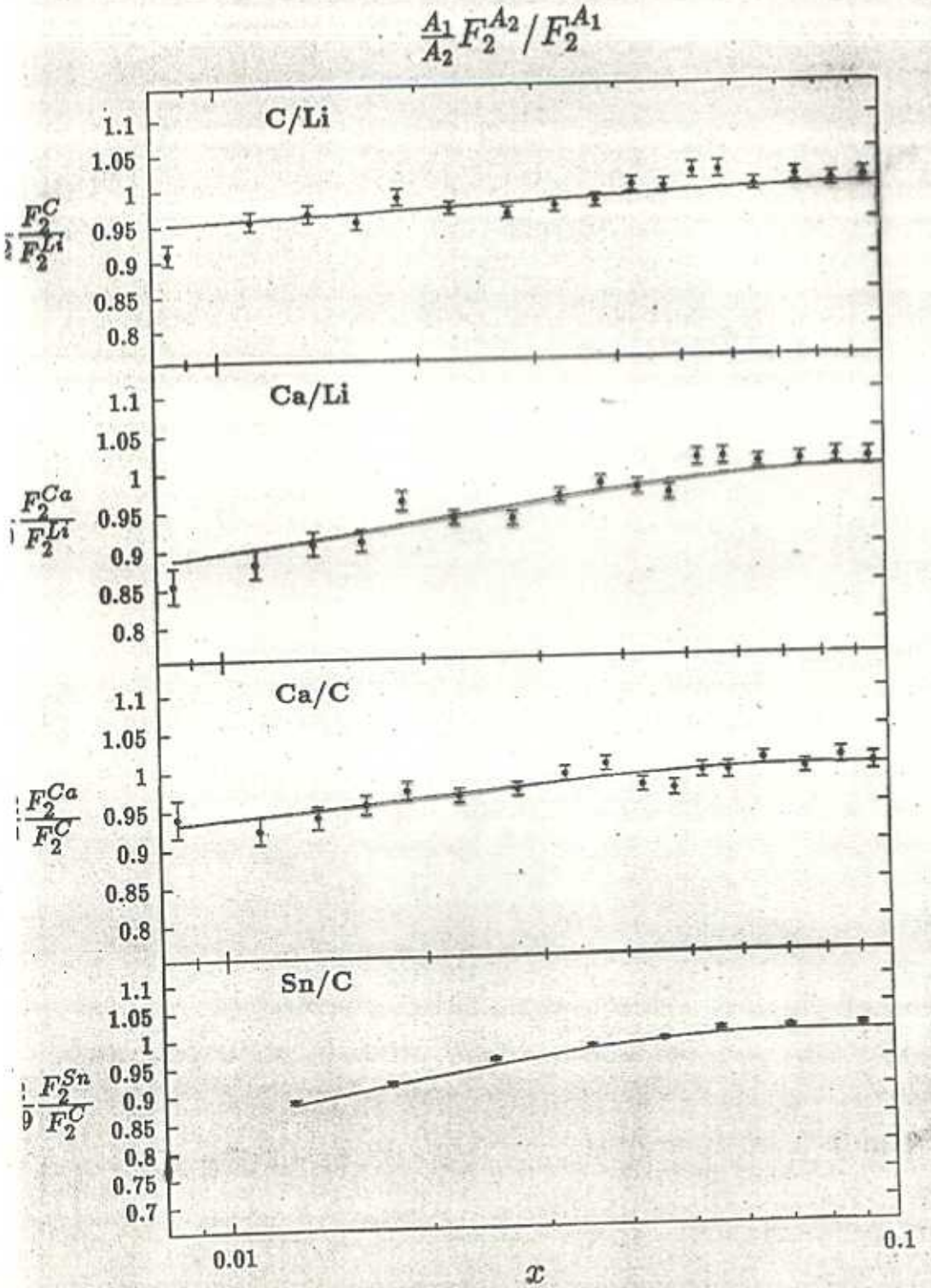
$\frac{A_1}{A_2} F_2^{A_2} / F_2^{A_1}$
C/Li
Ca/Li
Ca/C
Sn/C
$\frac{F_2^C}{F_2^{Li}}$
$\frac{F_2^{Ca}}{F_2^{Li}}$
$\frac{F_2^{Ca}}{F_2^C}$
$\frac{F_2^{Sn}}{F_2^C}$
1.1
1.05
1
0.95
0.9
0.85
0.8
0.75
0.7
0.01
0.1
x

Heavy ion collisions

The QCD Phase diagram.

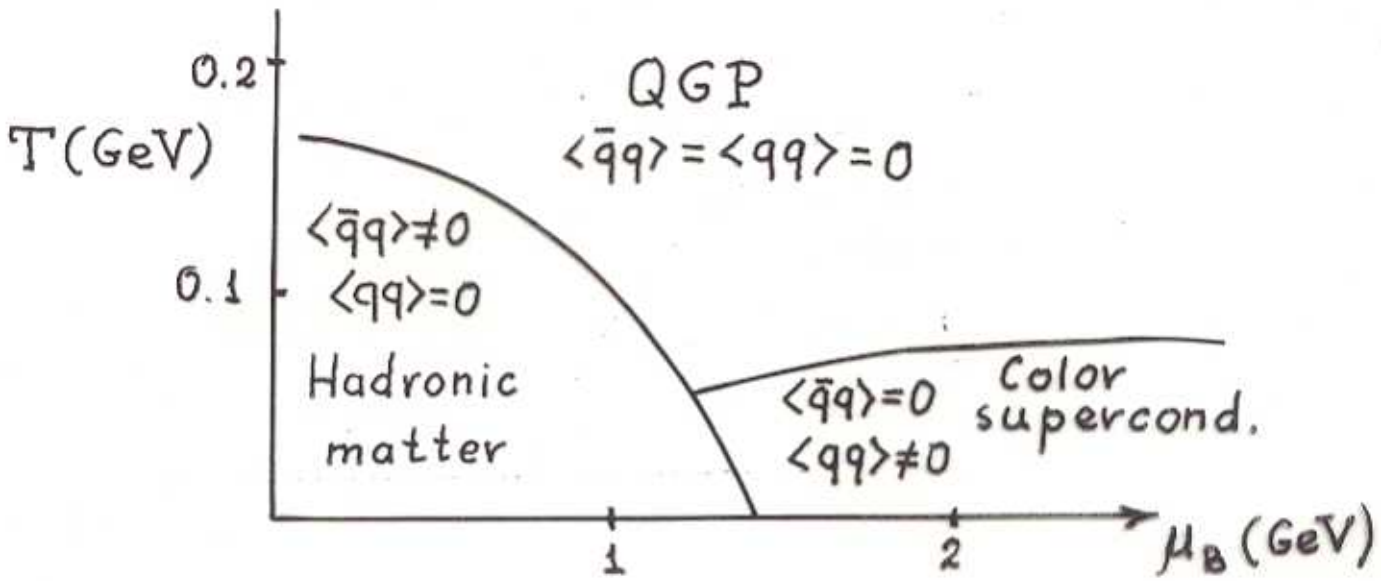

Confinement-deconfinement phase transition, chiral symmetry restoration.

Heavy ion collisions are considered as a tool to produce and study a new state of matter : the Quark Gluon Plasma (QGP).

Complicated structure of dense and hot quark-gluon matter above critical point. Difficult to formulate clear signals of QGP.

What are the initial states of colliding heavy ions at very high energies?

Interactions between partons with small x are important for high-energy heavy ion collisions.

The quark-gluon state corresponding to the "saturation" limit was called "The Color Glass Condensate" (McLerran et al.).

These effects lead to a substantial reduction of densities of hadrons produced in h.i. collisions compared to predictions of the model with independent interactions of nucleons (Glauber model)

This reduction is seen already at RHIC energies.

Table 1

Densities of charged hadrons $dn/d\eta|_{\eta=0}$ in central Pb-Pb collisions at $\sqrt{s} = 130\ GeV$.

Glauber	With shadowing corrections	Experimen
1200 ± 100	630 ± 120	555 ± 12

However the situation at RHIC is far from the saturation limit.

Experiments at RHIC observed a decrease of cross sections for production of particles and jets at large $p_\perp$. It can not be attributed to the shadowing of partons (at least in the central rapidity region: $x_i \sim 0.1$). This effect can be explained as a consequence of final state interactions (energy loss in a medium). Manifestation of QGP?

Jet quenching.

Very interesting are collective effects in nuclei. Any jet can be considered as a body fast moving in a medium. It induces some pressure in the nucleus. The "bounce-off" (the directed flow in the reaction plane) and "squeeze-out" (the second moment of the azimuthal particle emission distribution also called as elliptic flow) effects due to this pressure have been observed.

Mach waves can appear for jets moving with the speed exceeding that of sound. The specific two-maxima angular distributions of particles around the direction of propagation of jets have been measured. The similar effect can arise due to coherent Cherenkov gluons moving with the phase velocity lower than that of emitting it parton. The ring-like structure of particle emission in the plane perpendicular to the direction of propagation of jets has been seen. These effects are still waiting for more detailed QCD explanation. They should provide us the information about such properties of the quark-gluon matter as its index of nuclear refraction and speed of sound in it, which are deeply related to its equation of state.

Summary

The QCD perturbation theory is well developed at present and its predictions are in a good agreement with a vast amount of data on hard processes in e^+e^-, ep, $pp(p\bar{p})$, pA,.. collisions.

QCD is tested up to very small distances $\sim 10^{-17} cm$.